Energy Conversion and Management 198 (2019) 111776

Contents lists available at ScienceDirect

Energy Conversion and Management

journal homepage: www.elsevier.com/locate/enconman

# Preliminary experimental comparison and feasibility analysis of $CO_2$/R134a mixture in Organic Rankine Cycle for waste heat recovery from diesel engines

Peng Liu[a,b], Gequn Shu[a,*], Hua Tian[a,*], Wei Feng[b], Lingfeng Shi[a], Zhiqiang Xu[a]

[a] State Key Laboratory of Engines, Tianjin University, 92 Weijin Road, Nankai District, Tianjin 300072, China
[b] Energy Technologies Area, Lawrence Berkeley National Laboratory, 1 Cyclotron Road, Berkeley, CA 94720, USA

ARTICLE INFO

*Keywords:*
$CO_2$/R134a mixture
Experimental comparison
Feasibility analysis
Organic Rankine Cycle
Engine waste heat recovery

ABSTRACT

This paper presents results of a preliminary experimental study of the Organic Rankine Cycle (ORC) using $CO_2$/R134a mixture based on an expansion valve. The goal of the research was to examine the feasibility and effectiveness of using $CO_2$ mixtures to improve system performance and expand the range of condensation temperature for ORC system. The mixture of $CO_2$/R134a (0.6/0.4) on a mass basis was selected for comparison with pure $CO_2$ in both the preheating ORC (P-ORC) and the preheating regenerative ORC (PR-ORC). Then, the feasibility and application potential of $CO_2$/R134a (0.6/0.4) mixture for waste heat recovery from engines was tested under ambient cooling conditions. Preliminary experimental results using an expansion valve indicate that $CO_2$/R134a (0.6/0.4) mixture exhibits better system performance than pure $CO_2$. For PR-ORC using $CO_2$/R134a (0.6/0.4) mixture, assuming a turbine isentropic efficiency of 0.7, the net power output estimation, thermal efficiency and exergy efficiency reached up to 5.30 kW, 10.14% and 24.34%, respectively. For the fitting value at an expansion inlet pressure of 10 MPa, the net power output estimation, thermal efficiency and exergy efficiency using $CO_2$/R134a (0.6/0.4) mixture achieved increases of 23.3%, 16.4% and 23.7%, respectively, versus results using pure $CO_2$ as the working fluid. Finally, experiments showed that the ORC system using $CO_2$/R134a (0.6/0.4) mixture is capable of operating stably under ambient cooling conditions (25.2–31.5 °C), demonstrating that $CO_2$/R134a mixture can expand the range of condensation temperature and alleviate the low-temperature condensation issue encountered with $CO_2$. Under the ambient cooling source, it is expected that ORC using $CO_2$/R134a (0.6/0.4) mixture will improve the thermal efficiency of a diesel engine by 1.9%.

## 1. Introduction

World Energy Outlook in 2017 reported that China may become the world's largest oil importer in 2020 [1]. A major obstacle to reducing China's oil consumption is the growing demand of crude oil in the transportation sector. The crude oil consumed by internal combustion engines (ICEs) accounts for 60% of China's total crude oil consumption [1]. Constrained by the structure of the ICE and the Carnot cycle efficiency, more than half of the combustion heat of an internal combustion engine is discharged through various forms of waste heat. Hence, waste heat recovery (WHR) technologies are regarded as a promising way to improve the fuel efficiency of ICEs and thus to reduce China's oil consumption. Among technologies, Organic Rankine Cycle (ORC) is considered suitable for ICE-WHR because of its high efficiency, suitable system size and low impact on the ICE itself [2].

The choice of working fluid is critical for using an ORC system for ICE-WHR. Recent research has examined traditional refrigerant-based ORC systems in terms of integration optimization [3], selection of working fluid [4], configuration comparison [5] and dynamic performance [6]. However, traditional refrigerants, including CFCs, HCFCs and HFCs, contribute significantly to climate change and global warming [7]. The global warming potential (GWP) and ozone depletion potential (ODP) of such refrigerants are higher than those of $CO_2$. Various protocols and amendments have been established to control and limit the use and production of traditional refrigerants. Recently, governments around the world introduced a phase-out plan for CFCs and HCFCs and use limitations for HFCs [8]. It is important, therefore, to investigate alternative working fluids that have zero GWP and ODP.

This paper is organized as follows: A literature review is presented in Section 2. Section 3 gives a brief description of the ORC test bench used in the current study. Section 4 discusses the selection of working fluids. The experimental strategy is presented in Section 5. Section 6

* Corresponding authors.
*E-mail addresses:* sgq@tju.edu.cn (G. Shu), thtju@tju.edu.cn (H. Tian).

https://doi.org/10.1016/j.enconman.2019.111776
Received 23 April 2019; Received in revised form 28 June 2019; Accepted 1 July 2019

**Nomenclature**

| | |
|---|---|
| $c_p$ | Specific heat (kJ/kW K) |
| $E$ | Exergy flow rate (kW) |
| $h$ | Enthalpy (kJ/kg) |
| $I$ | Exergy destruction (kW) |
| $m$ | Mass flow rate (kg/s) |
| $P$ | Pressure (MPa) |
| $Q$ | Heat flow rate (kW) |
| $T$ | Temperature (°C) |
| $W$ | Power output (kW) |
| $\eta$ | Efficiency (%) |
| $\Delta T_{lm}$ | Log mean temperature difference (°C) |
| *is* | Isentropic |
| *in* | Inlet |
| *max* | Maximum |
| *net* | Net power |
| *out* | Outlet |
| *p* | Pump |
| *pre* | Preheater |
| *reg* | Regenerator |
| *t* | Turbine |
| *th* | Thermal |

*Subscripts*

| | |
|---|---|
| *con* | Condenser |
| *cw* | Cooling water side |
| *1–9* | Work fluid state point |
| *ave* | Average |
| *eg* | Exhaust gas side |
| *ex* | Exergy |
| exp | Expansion process |
| *est* | Estimation |
| *f* | Working fluid |
| *gh* | Gas heater |

*Abbreviations*

| | |
|---|---|
| CW | Cooling water |
| EC | Engine coolant |
| EG | Exhaust gas |
| ICE | Internal combustion engine |
| ORC | Organic Rankine Cycle |
| P-ORC | Preheating Organic Rankine Cycle |
| PR-ORC | Preheating regenerative Organic Rankine Cycle |
| PR | Pressure ratio |
| RD | Relative difference |
| WHR | Waste heat recovery |

describes the experiments conducted to compare performance of working fluids and to perform feasibility analysis. Major conclusions are summarized at the end of the paper. The originality of this paper centers on three primary features.

1. This paper presents the first experimental results for an ORC system that uses $CO_2$/R134a mixture.
2. This paper describes the first attempt to conduct an experimental comparison between a $CO_2$/R134a mixture and pure $CO_2$ in an ORC system and to demonstrate the performance improvement obtained by $CO_2$/R134a mixture.
3. Experimental results under ambient cooling conditions indicate that $CO_2$/R134a mixture can expand the range of condensation temperatures and alleviate the issue of the low-temperature condensation encountered with $CO_2$.

## 2. Literature review

In several earlier investigations of ORC-based ICE-WHR, the $CO_2$ transcritical Rankine cycle (TRC) showed great potential [9–11]. First, $CO_2$ is environmentally friendly, non-toxic, non-flammable and inexpensive. In addition, $CO_2$ provides heat stability adequate to withstand the high temperatures of the exhaust gas from ICEs. Secondly, previous studies indicated that $CO_2$ is capable of utilizing heat from exhaust gas and engine coolant simultaneously and has a good thermal matching, reducing irreversible losses occurred during the heating process [9,12]. Finally, $CO_2$ supports the miniaturization of ORC systems: $CO_2$ turbines are expected to be small and simple, and $CO_2$ holds promise for use with compact microchannel heat exchangers [13,14]. Byung Chul Choi [15] presented a $CO_2$-TRC with two-stage reheat to recover waste heat from the jacket water and the intercooler, revealing that the maximum cycle efficiency is 9.26%. Wang et al. [16] compared three configurations of $CO_2$ based TRC concluding that the single stage cycle is preferable when the exhaust gas temperature is 300 °C–600 °C. Experimental analysis conducted by the Echogen Power Company [17] indicated that $CO_2$-based TRC achieved higher efficiency than organic or steam-based Rankine cycle within a wide temperature range and for a small system. Previous experiments conducted by our group demonstrated that $CO_2$ based TRC could not only improve the thermal efficiency and reduce the cooling load of the diesel engine [11], but also possesses good dynamic characteristics [18–20].

Because of the low critical temperature, however, it is difficult for $CO_2$ to be condensed into a liquid state under the ambient cooling conditions. This difficulty presents an obstacle to the practical application of a $CO_2$ based TRC, especially for WHR for vehicles. Meanwhile, $CO_2$ based TRC provides relatively low thermal efficiency because of the corresponding small pressure ratio. To alleviate the disadvantages noted above, some researchers have explored the feasibility of using $CO_2$ mixtures [21–25]. Shu et al. [22] investigated the performance improvement by using $CO_2$ mixture in transcritical Rankine cycle for WHR of a diesel engine. The results indicated that $CO_2$ mixture can improve system performance, expand the range of condensation temperature and decrease operating pressure. Dai et al. [23] studied the seven $CO_2$ mixtures in low temperature TRC, revealing that such mixtures are capable of improving thermal efficiency and reducing operating pressure in comparison of $CO_2$. Wu et al. [24] compared various $CO_2$-based mixtures for the energy conversion of geothermal water, demonstrating that $CO_2$-based mixtures achieve superior thermo-economic performance although they require a larger heat transfer area. Yin et al. [26] investigated the supercritical/transcritical Rankine cycle for geothermal power plants, using a $CO_2/SF_6$ mixture and determining the optimal concentration of $SF_6$.

Despite some previous research, there are few reported experiments that incorporate $CO_2$ mixtures into ORC. Indeed, published results of ORC experiments using a $CO_2$ mixture as the working fluid are extremely rare because of safety concerns, insufficient experience and industrial confidentiality [27]. Wang et al. [28] presented an experimental study of a low-temperature solar ORC using R245fa/R152a mixture as working fluid, indicating that R245fa/R152a mixture showed the potential to improve overall efficiency. An experimental comparison between the R245fa/R134a mixture and pure R245fa in a low-temperature small-scale ORC was conducted by Bamorovat Abadi et al. [29]. The results showed that R245fa/R134a mixture performed well with heat source temperatures ranging from 80 °C to 100 °C and the mixture achieved higher power output at a lower pressure ratio. Jung et al. [30] used an ORC test rig to examine the dynamic behavior

of R245fa/R356mfc. Li et al. [31] conducted a performance comparison between R245fa and a R245fa/R601a mixture in the ORC system and concluding that the R245fa/R601a mixture improved the heat transfer performance of the vapor generator and obtained higher thermal efficiency. Pang et al. [32] examined the maximum net power output of an ORC system for industrial waste heat using R245fa, R123 and their mixtures.

Our literature review revealed that previous experimental research into using $CO_2$ mixtures for ORC focused primarily on the refrigerant/refrigerant mixtures, which have contributed to the application of low-temperature ORC. Lacking are experimental results for $CO_2$ mixtures in high-temperature ORC applications. In addition, there are almost no experimental results to assess the feasibility of using $CO_2$/R134a mixtures to expand the range of condensation temperatures, which is required for using ICE-WHR in vehicles.

This paper describes a preliminary experimental study using an expansion valve in a small-scale ORC test bench coupled with a heavy-duty diesel engine. Exhaust gas and engine coolant were utilized as heat sources for the ORC test bench. Measured operating parameters as well as system performance of pure $CO_2$ and a $CO_2$/R134a mixture (0.6/0.4 on a mass basis) were compared under both a P-ORC and a PR-ORC. System performance using a $CO_2$/R134a mixture under ambient cooling conditions also was analyzed.

## 3. Description of test bench

A small-scale Organic Rankine Cycle (ORC) test bench was built to recover waste heat from the exhaust gas and engine coolant of a diesel engine. The entire test bench comprises the diesel engine, the ORC system and the cooling system. Measurement devices including pressure transmitter, thermocouple and flow transmitter are installed in the test bench. Fig. 1 presents a schematic diagram of the ORC test bench and indicates the location of each measurement point. Fig. 2 is a photo of the ORC test bench.

The engine used in the experiment is a heavy duty, 6-cylinder, 4-stroke diesel engine (parameters are detailed in Table 1). The diesel engine is equipped with a system that can be used to control and record the diesel engine's operating conditions. A water tank is provided in lab to supply engine coolant for the diesel engine, and the flow rate of engine coolant is controlled by pump (EC Pump 1 in Fig. 1). Another engine coolant pump (EC Pump 2 in Fig. 1) is installed to drive part of the engine coolant as the preheating source for the ORC system.

The cooling system provides a steady cooling water source (5 °C – 12 °C) for the ORC system. Most of the cooling water is used to cool the working fluid in the condenser to ensure that it is in a liquid state when it flows into the liquid receiver. To prevent possible gasification of the working fluid during pressurization of the working fluid plunger pump, another small portion of the cooling water is used to cool the plunger pump head and the liquid receiver.

The ORC system consists of the preheater, regenerator, gas heater, expansion valve, control valves, condenser-1, condenser-2, plunger pump and some measurement devices. A self-made double-pipe type heat exchanger is used for the gas heater, since it must withstand both high temperature and high pressure. Brazed plate heat exchangers, supplied by SWEP, is used for the preheater, the regenerator and the condensers, considering the system compactness. The flow rate of the working fluid for the ORC system is controlled by a reciprocating plunger pump (model 3RC50A-1.7/12). The liquid receiver is designed and manufactured as a vertical cylindrical barrel with a volume of 10L. A magnetic flip plate type level sensor installed in the liquid receiver shows the change of liquid height in the receiver. There is a lack of corresponding experiment results about $CO_2$ mixture, considering the possible turbine damage caused by the refrigerant component in $CO_2$/R134a mixture, a home-made expander valve is temporarily used to replace the expander in the current studies. By controlling the opening degree of the expander valve, we can estimate and analyze system performance under various expansion inlet pressures.

The experimental bench is unique in that the preheating ORC (P-ORC) system and preheating regenerative ORC (PR-ORC) system can easily be switched by controlling valves 1 through 6. Closing valves 2 through 5 and opening valves 1 and 6 imitates a P-ORC system. Conversely, closing valves 1 and 6 and opening valves 2 through 5 imitates a PR-ORC system.

Measuring instruments such as pressure sensors, temperature sensors and flow meters are installed on the test bench, as shown in Fig. 1. A data collection module performs data acquisition and conversion, then connects to a computer through an RS232 communication cable. The overall performance of the system can be determined by measuring the thermodynamic states at each measurement point. Using the error analysis method described in our previous publication [18], the

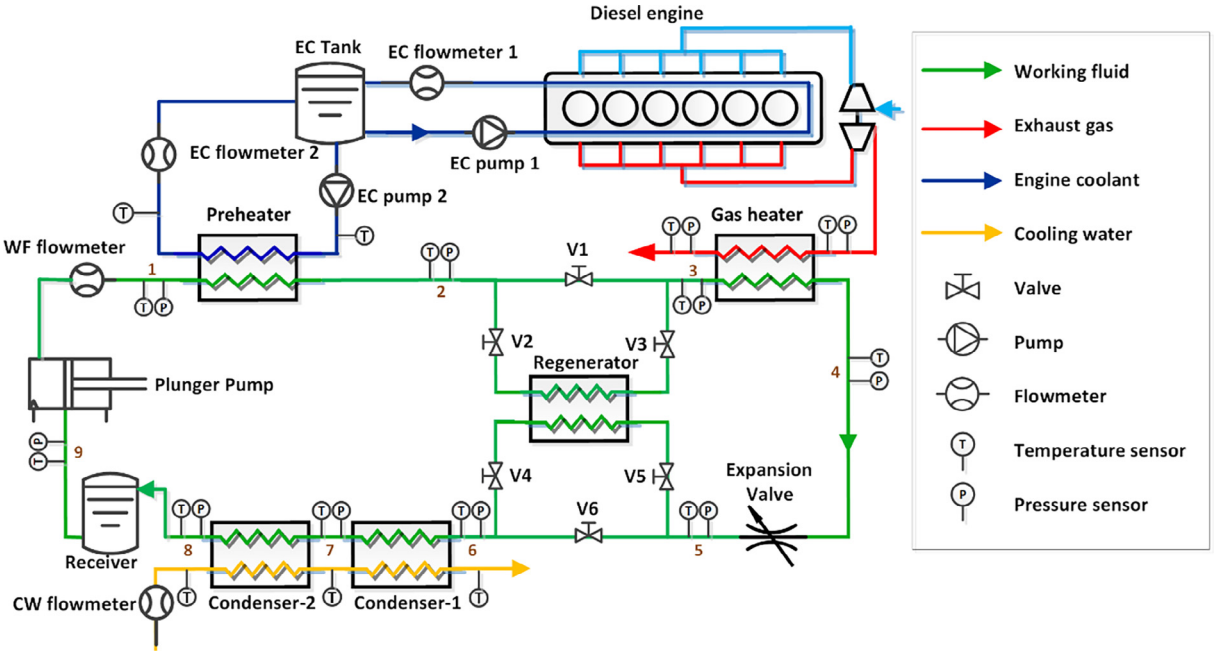


**Fig. 1.** Schematic diagram of the ORC test bench and the location of each measurement point.

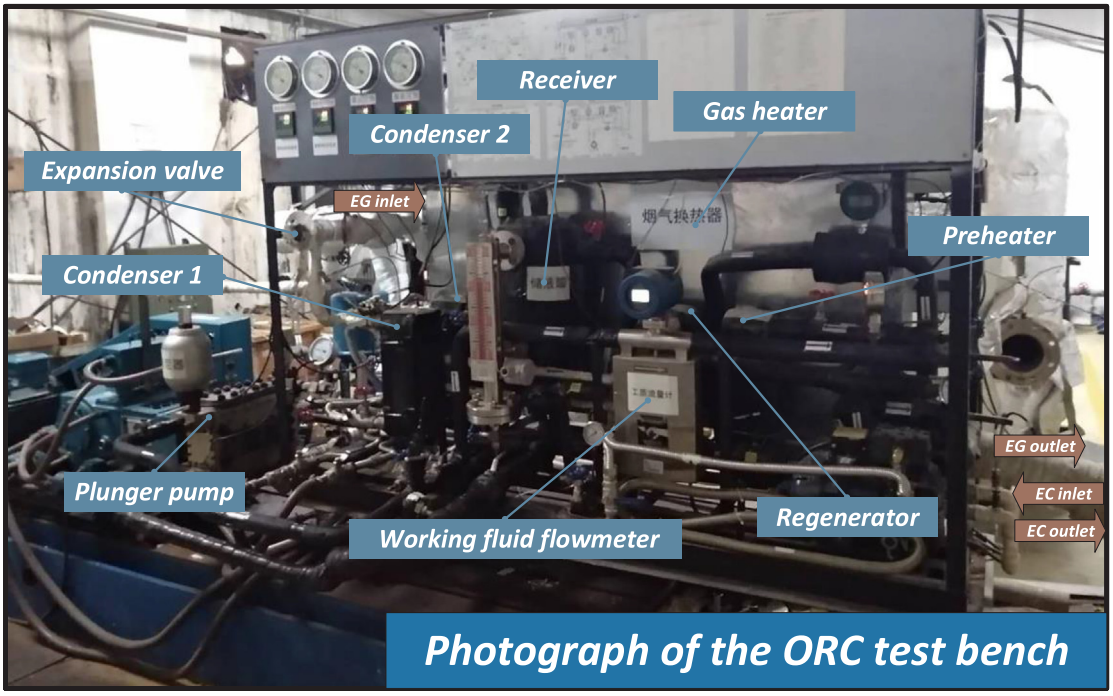


**Fig. 2.** Photograph of the ORC test bench.

**Table 1**
Specifications for diesel engine in test bench.

| Parameter | Units | Description |
|---|---|---|
| Engine Type | – | In-line, 4 Stroke |
| Cylinder number | – | 6 |
| Bore × Stroke | mm × mm | 113 × 140 |
| Displacement | L | 8.424 |
| Intake model | – | Supercharged and intercooling |
| Fuel injection | – | High pressure common rail |
| Maximum torque | N m | 1280@1200–1700 rpm |
| Rated Speed | rpm | 2200 |
| Rated power | kW | 243 |

maximum relative uncertainties of $Q_{gh,f}$, $Q_{gh,eg}$ and $Q_{con,cw}$ are 1.1%, 5.71% and 2.0%, respectively. Specifications and uncertainties of measuring devices are listed in Table 2.

## 4. Selection of working fluid

Previous studies have analyzed and discussed the theoretical thermodynamic performance of the ORC using mixtures composed of $CO_2$ and other refrigerants. To allow for condensation at ambient temperatures in practical applications, the refrigerant additive should have a higher critical temperature than $CO_2$. Moreover, the refrigerant additive should have good safety and environmental characteristics. Because it is non-flammable, has zero ODP and a low GWP, R134a is widely used as a high-temperature refrigerant in automobile air conditioners [33], which indicate R134a hold great potential to be used for other application in automobile field. Previous theoretical analysis conducted by our group [22] showed that $CO_2$/R134a mixture has moderate temperature glide and good thermodynamic performance. Ref. [22] also concludes that $CO_2$/R134a mixture with an approximate 40%～50% mass fraction of R134a may produce superior system performance. Thus, we selected the mixture of $CO_2$/R134a (0.6/0.4) on a mass basis for comparison with pure $CO_2$. The major physical parameters of pure $CO_2$, R134a and $CO_2$/R134a mixture are listed in Table 3. Fig. 3 shows the *T-s* diagram of $CO_2$/R134a (0.6/0.4) mixture and pure $CO_2$. It is clear that $CO_2$/R134a (0.6/0.4) mixture owns higher critical temperature and critical pressure in comparison with $CO_2$. It should be noted that the thermodynamic properties of the working fluid were obtained using REFPROP 9.0.

## 5. Experimental strategy and evaluation model

### 5.1. Experimental strategy

This paper describes the experimental approach in two parts. First, the performance of the $CO_2$/R134a mixture is evaluated and compared with that of pure $CO_2$ in the P-ORC and PR-ORC. Then, after shutting down the refrigerating unit, another experimental test is conducted under ambient cooling conditions to demonstrate the feasibility and

**Table 2**
Specifications and accuracies of the test bench measuring devices.

| Measuring device | Type | Range | Accuracy |
|---|---|---|---|
| *Flow rate* | | | |
| Engine intake air flowmeter | Laminar flow | 0–1350 kg/h | ± 0.5% |
| Fuel consumption meter | – | 5–2000 kg/h | – |
| $CO_2$ flowmeter | Coriolis type | 0–1080 kg/h | ± 0.2% |
| EC flowmeter1 | Turbine | 2–40 $m^3$/h | ± 0.5% |
| EC flowmeter2 | Turbine | 0–10 $m^3$/h | ± 0.5% |
| Cooling water flowmeter | Turbine | 0–12 $m^3$/h | ± 1% |
| *Liquid level* | | | |
| $CO_2$ liquid level meter | Magnetic flap type | 0–30 cm | ± 3.3% |
| *Temperature* | | | |
| Temperature sensor for EG | Thermocouple type | −60–650 °C | ± 1% |
| Temperature sensor for others | Thermo-resistive type | −200–500 °C | ± 0.15% |
| *Pressure* | | | |
| Pressure transmitter for EG and CW | Low pressure type | 0–0.5 MPa | ± 0.065% |
| Pressure transmitter for low pressure $CO_2$ | Low pressure type | 0–12 MPa | ± 0.065% |
| Pressure transmitter for high pressure $CO_2$ | High pressure type | 0–14 MPa | ± 0.065% |

**Table 3**
Properties of $CO_2$, R134a and $CO_2$/R134a (0.6/0.4) mixture.

| | $CO_2$ | R134a | $CO_2$/R134a (0.6/0.4) |
|---|---|---|---|
| Molecular mass (g/mol) | 44.01 | 102.03 | 67.22 |
| Critical temperature (°C) | 31.1 | 101.1 | 58.3 |
| Critical pressure (MPa) | 7.38 | 4.06 | 7.80 |
| ODP | 0 | 0 | – |
| GWP | 1 | 1300 | – |
| ASHRAE 34 safety group | A1 | A1 | – |

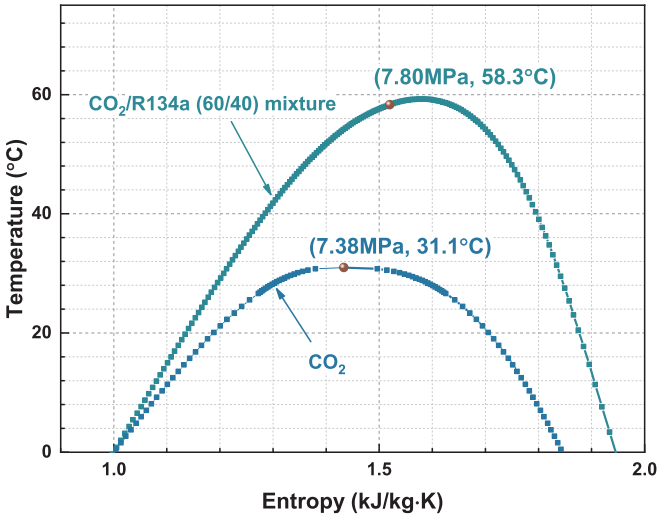


**Fig. 3.** *T-s* diagram of $CO_2$/R134a (0.6/0.4) mixture and pure $CO_2$.

potential of the $CO_2$/R134a mixture for waste heat recovery from vehicle engines.

To perform a reasonable comparison between pure $CO_2$ and the $CO_2$/R134a mixture, the diesel engine operates under the same working conditions for both (50% load at 1100 rpm), which is the medium duty of the diesel engine used in the test. Even if the diesel engine runs at a constant operating point, clearly the temperature and flow rate of waste heat sources may fluctuate in response to factors such as changes in environmental conditions or unsteady engine operation. Table 4 shows the operating parameters and waste heat source parameters for the diesel engine used in the experiments, as well as the maximum relative difference ($RD_{max}$) of each parameter. The maximum relative differences are obtained based on the engine coolant flow rate due to fluctuations in the level of liquid in the water tank. Except for the engine coolant flow rate, the maximum relative differences of parameters are within 5%. The difference in heat sources caused by the unsteady operation of the diesel engine is acceptable in this comparative experiment.

Experimental strategy is described briefly here. First, some preparation work must be done, such as checking the seals in the ORC bench and verifying the position of valves and the functioning of refrigeration unit. Then, the diesel engine is started and warmed up. Testing with the ORC test bench begins when the temperature of the exhaust gas reaches 180 °C. The speed and load of the diesel engine as well as the mass flow rate of the working fluid are increased gradually to their set points. As mentioned above, the set operating conditions of the diesel engine are 600 N m and 1100 rpm. The flow rate of the working fluid is set to 11.5 ± 0.2 kg/min. After the diesel engine and the ORC test bench are operating consistently, the expansion valve opening is reduced manually to create sub-scenarios involving various pressures on ORC system. This way, the system performance of pure $CO_2$ and of $CO_2$/R134a mixture can be compared preliminarily under various pressures. During the experimental process, for safety reasons the maximum pressure of the ORC test bench cannot exceed 11 MPa. It should be noted that those experiments were performed at different time, so that the temperatures of the cooling water differed slightly because it was affected by the ambient temperature. Table 5 gives the cooling conditions for the various tests.

**Table 5**
Cooling conditions for different working fluids and modes.

| | Pure $CO_2$ | | $CO_2$/R134a mixture | |
|---|---|---|---|---|
| | P-ORC | PR-ORC | P-ORC | PR-ORC |
| Cooling water temperature (°C) | 7.6–7.8 | 7.1–7.9 | 9.4–9.5 | 9.4–9.4 |
| Cooling water mass flow rate ($m^3$/h) | 1.87–1.89 | 1.93–1.94 | 1.92–1.93 | 1.92–1.92 |

### 5.2. Evaluation model

Based on the measured parameters, we estimated the thermodynamic performance of the system, including net output work, thermal efficiency and exergy efficiency. MATLAB 2015 software was used to establish the mathematic models. The mathematical equations for each component and for system performance are described below.

The amount of heat absorbed by the working fluid during the heating process—in the preheater, the regenerator and the gas heater—can be calculated as follows.

$$\dot{Q}_{pre} = \dot{m}_f (h_2 - h_1) \quad (1)$$

$$\dot{Q}_{reg} = \dot{m}_f (h_3 - h_2) \quad (2)$$

$$\dot{Q}_{gh} = \dot{m}_f (h_4 - h_3) \quad (3)$$

Because the radial flow turbine is unfinished, in the test bench the expansion valve is used temporarily in place of the expander. With the measured parameters of expansion inlet temperature, expansion inlet pressure and expansion outlet pressure, the net power output can be estimated by assuming a constant isentropic expansion efficiency as

**Table 4**
Engine operating parameters and heat source conditions for various experimental scenarios and maximum relative differences of parameters.

| | Pure $CO_2$ | | $CO_2$/R134a mixture | | $RD_{max}$ |
|---|---|---|---|---|---|
| Parameter | P-ORC | PR-ORC | P-ORC | PR-ORC | |
| Engine speed (rpm) | 1100 | 1106 | 1099 | 1098 | 0.5% |
| Engine torque (N m) | 594 | 603 | 601 | 601 | 1.0% |
| Power output (kW) | 68.2 | 69.7 | 68.8 | 68.8 | 1.2% |
| BSFC (g/kWh) | 215.2 | 228.2 | 221.8 | 221.8 | 3.0% |
| Exhaust gas temperature (°C) | 489.3–501.0 | 490.6–506.6 | 490.7–493.7 | 494.4–496.0 | 2.1% |
| Exhaust gas mass flow rate (kg/h) | 320.6–323.4 | 316.0–321.1 | 325.6–328.5 | 323.9–326.2 | 2.1% |
| Engine coolant temperature (°C) | 71.3–75.7 | 71.3–72.3 | 69.9–73.5 | 70.8–73.4 | 5.0% |
| Engine coolant mass flow rate ($m^3$/h) | 0.23–0.24 | 0.24–0.25 | 0.23–0.27 | 0.24–0.26 | 10.2% |

$RD_{max} = | X - X_{ave} |_{max}/X_{ave}$.

follows [11,34].

$$\dot{W}_p = \dot{m}_f (h_1 - h_9) \tag{4}$$

$$\dot{W}_{exp,est} = \dot{m}_f (h_4 - h_5) \tag{5}$$

$$h_5 = h_4 - (h_4 - h_{5,ideal})\eta_{exp} \tag{6}$$

$$\dot{W}_{net,est} = \dot{W}_{exp,est} - \dot{W}_p \tag{7}$$

wherein $h_{5,ideal}$ is the ideal enthalpy of state 5, assuming that the working fluid expands from state 4 to state 5 in an isentropic process. $h_5$ is the enthalpy at state 5 with the consideration of irreversible loss in expansion process. The isentropic efficiency of the expander is assumed to be 70%, which is the target value when manufacturing turbine and also is reasonable for current $CO_2$ power cycle applications [35].

The thermal efficiency of the ORC system is defined as follows.

$$\eta_{th} = \frac{\dot{W}_{net,est}}{\dot{Q}_{pre} + \dot{Q}_{gh}} \tag{8}$$

The exergy destruction in each heat exchanger and the exergy efficiency are calculated by:

$$\dot{I}_{pre} = (\dot{E}_{EC,in} - \dot{E}_{EC,out}) - (\dot{E}_2 - \dot{E}_1) \tag{9}$$

$$\dot{I}_{reg} = (\dot{E}_5 - \dot{E}_6) - (\dot{E}_3 - \dot{E}_2) \tag{10}$$

$$\dot{I}_{gh} = (\dot{E}_{EG,in} - \dot{E}_{EG,out}) - (\dot{E}_4 - \dot{E}_3) \tag{11}$$

$$\dot{I}_{con1+con2} = (\dot{E}_6 - \dot{E}_8) \tag{12}$$

$$\eta_{ex} = \frac{\dot{W}_{net,est}}{(\dot{E}_{EC,in} - \dot{E}_{EC,out}) + (\dot{E}_{EG,in} - \dot{E}_{EG,out})} \tag{13}$$

## 6. Results and discussion

During the experiments, the measured parameters, including temperature, pressure and flow rate at each measurement point, are recorded automatically. Before evaluating system performance, we compared the measured operating parameters between pure $CO_2$ and $CO_2$/R134a mixture. Subsequently, system thermodynamic performance was discussed.

### 6.1. Comparison of operating parameters of pure $CO_2$ and $CO_2$/R134a mixture

At the beginning of the experiment, the flow rate of the working fluid flow rate was gradually increased to the set value. This process took about 40 min. The data collected for pure $CO_2$ and $CO_2$/R134a mixture are shown in Fig. 4. As noted, the $CO_2$ flow rate was increased steadily after the period of flow fluctuation when the working fluid pump started. However, the ORC system using $CO_2$/R134a mixture underwent drastic flow fluctuations over a long period, which could be caused by the unevenness of the mixture. After the $CO_2$/R134a mixture mixed evenly, the flow rate remained consistent throughout the experiment. Hence, preparation work is recommended to ensure complete mixing of $CO_2$/R134a mixture when used as the working fluid of an ORC.

Tests were begun after the ORC test bench and diesel engine operated steadily. Fig. 5 shows the variation of expansion inlet and outlet pressures over time for the PR-ORC system. Each step change of pressure means a decrease in valve opening. For pure $CO_2$, 11 steady operating points, corresponding to expansion inlet pressures ranging from 6.8 to 10.7 MPa, were selected for analysis and comparison. 9 steady operating points, corresponding to expansion inlet pressures ranging from 5.2 to 10.6 MPa, were chosen for $CO_2$/R134a mixture. As shown in Fig. 5, the expansion outlet pressure when using $CO_2$/R134a mixture is significantly lower than that when using pure $CO_2$. This difference is attributable to the fact that $CO_2$/R134a mixture exhibits a lower saturated pressure than pure $CO_2$ at the same temperature. As a consequence, the pressure ratios of $CO_2$/R134a mixture are larger than those of pure $CO_2$, which also are noted in Fig. 5.

Expansion inlet pressure was selected as the indicator for detecting steady state in an ORC system [18]. As shown in Fig. 5, the entire ORC system operates steadily within 2–3 min before the expansion valve opening is changed again. Steady state points within 20 s before the next change of expansion valve are used for performance analysis.

Temperature variation at each measurement point directly reflects the heat recovery capacity of an ORC system. Fig. 6 shows the variation in temperature with expansion inlet pressure at the preheater outlet ($T_2$), the regenerator outlet ($T_3$) and the gas heater outlet ($T_4$). For both pure $CO_2$ and $CO_2$/R134a mixture, $T_2$ and $T_3$ demonstrate a trend of increasing with expansion inlet pressure. Meanwhile, the temperatures of pure $CO_2$ at points 2 and 3 are always lower than those of $CO_2$/R134a mixture. This finding can be explained by the fact that pure $CO_2$ is capable of absorbing more heat per mass at low-medium temperatures, reflected by larger specific heat capacity, as shown in Fig. 7. A further finding is that as the expansion inlet pressure increases, the $T_4$ for $CO_2$ increases from 181.6 °C to about 200 °C, while the $T_4$ of $CO_2$/R134a mixture decreases from 188.5 °C to 175.2 °C. The reversed temperature trends for pure $CO_2$ and $CO_2$/R134a mixture result from the combination of two actions: (a) the mass flow rate of the working fluid decreases due to the throttle effect of the expansion valve, producing the increase in $T_4$ for both $CO_2$ and the $CO_2$/R134a mixture; and (b) the specific heat of the $CO_2$/R134a mixture in the exhaust gas recovery zone increases with pressure (Fig. 7(b)), indicating that the $CO_2$/R134a mixture can absorb more heat per mass than pure $CO_2$. A greater capacity for heat absorption results in the decrease in $T_4$. Conversely, no sensible change in specific heat in the exhaust gas recovery zone was seen for $CO_2$ (Fig. 7(a)).

### 6.2. Comparison of the performance of pure $CO_2$ and $CO_2$/R134a mixture

The aim of this section is to examine and compare the system performance of pure $CO_2$ and $CO_2$/R134a (0.6/0.4) mixture in an ORC system. First, we discuss the difference in the capacity for waste heat recovery. Fig. 8 shows the amount of heat absorption for pure $CO_2$ and

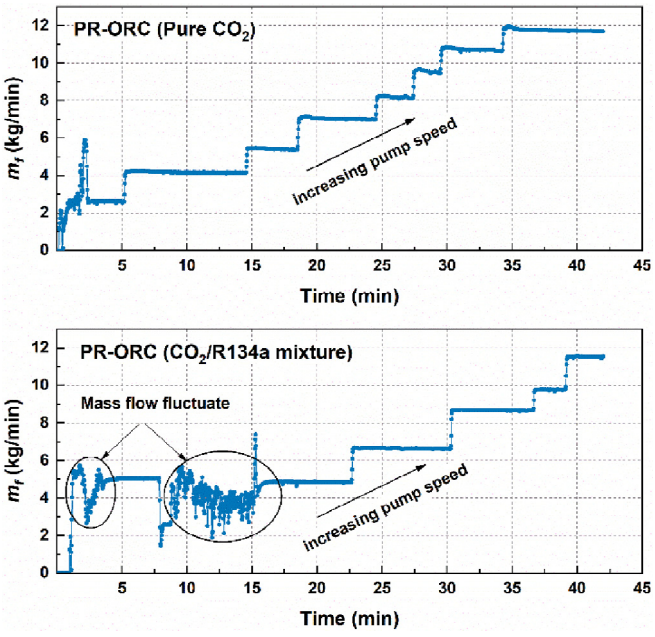


**Fig. 4.** Variation in flow rate of the working fluid at the beginning of experiment.

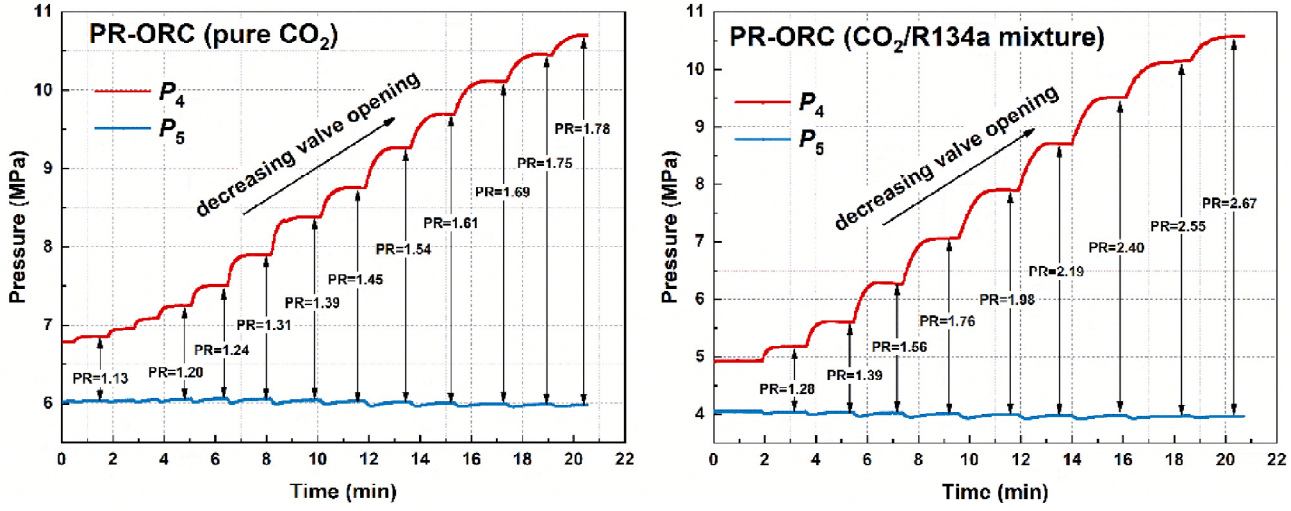


**Fig. 5.** Variation in expansion inlet and outlet pressures over time for the PR-ORC.

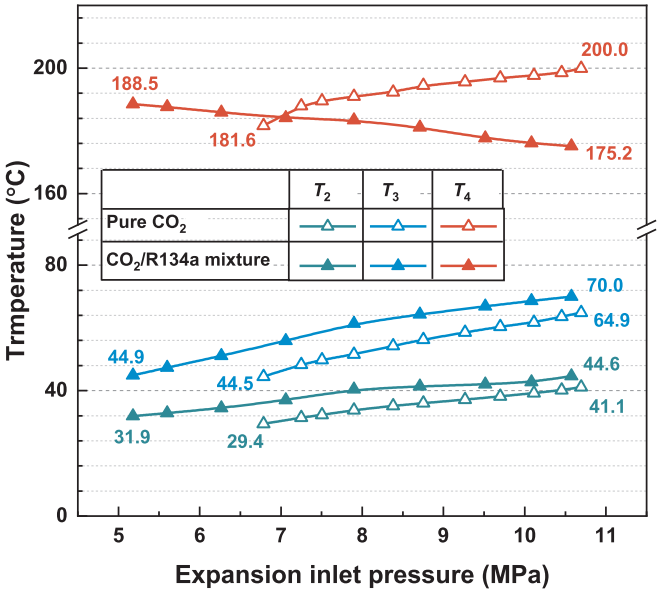


**Fig. 6.** Variation in temperature at the preheater outlet ($T_2$), regenerator outlet ($T_3$) and gas heater outlet ($T_4$) with expansion inlet pressure.

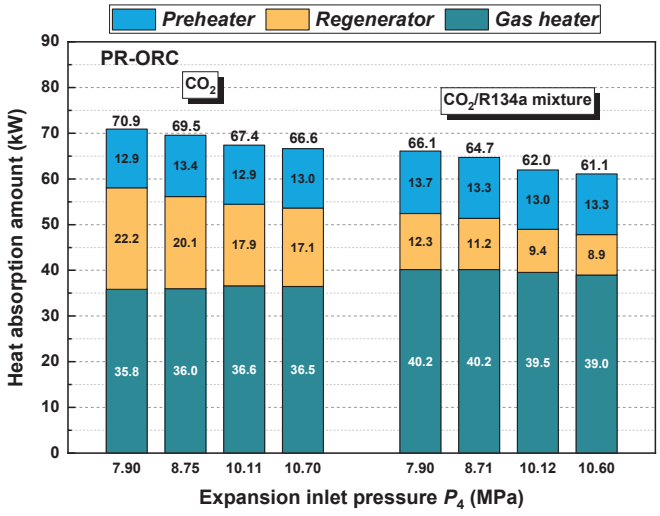


**Fig. 8.** Amount of heat absorption by pure $CO_2$ and $CO_2$/R134a mixture in the PR-ORC.

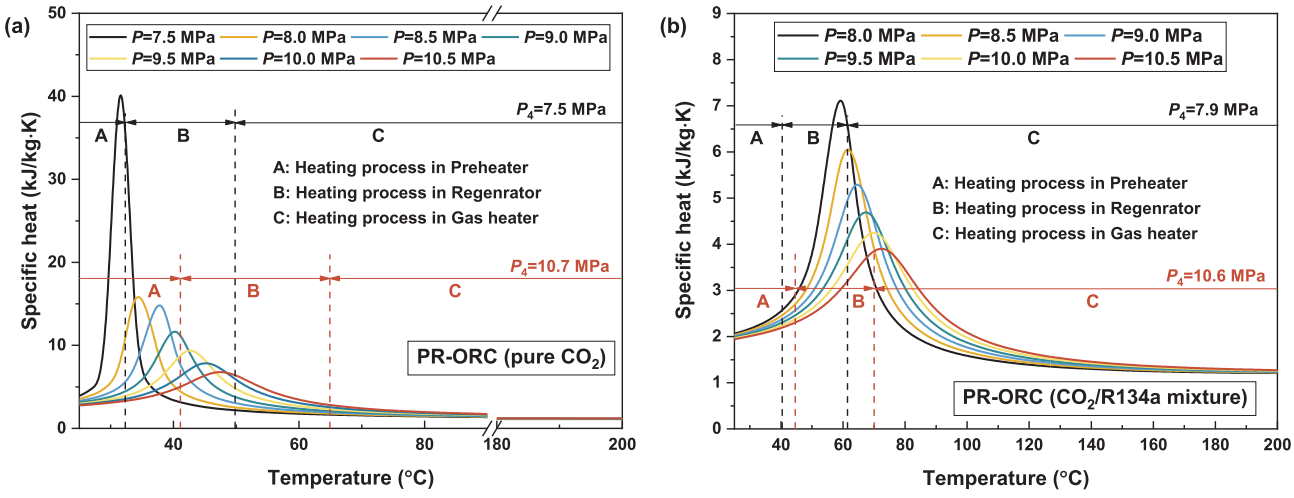


**Fig. 7.** Variation in specific heat capacity under various pressures. (a) pure $CO_2$; (b) $CO_2$/R134a mixture.

$CO_2$/R134a mixture in the PR-ORC system. On the whole, pure $CO_2$ is capable of absorbing more heat than $CO_2$/R134a mixture. Compared to pure $CO_2$, $CO_2$/R134a mixture recovers more heat from the exhaust gas, which is attributed to the high $c_p$ in the exhaust gas recovery zone of $CO_2$/R134a mixture (as shown in Fig. 7). Additionally, the amount of regeneration is significantly lower for $CO_2$/R134a mixture than for pure $CO_2$ because during the expansion process $CO_2$/R134a mixture accommodates a higher pressure drop and larger enthalpy difference.

Fig. 9 depicts the relationship between the net power output estimation and the expansion inlet pressure. As expected, for both pure $CO_2$ and $CO_2$/R134a mixture, the net power output estimations of the P-ORC and the PR-ORC display upward trend. However, $CO_2$/R134a mixture yields more net power output than pure $CO_2$ in both the P-ORC and the PR-ORC. The higher net power outputs achieved by $CO_2$/R134a mixture are attributed to its lower condensation pressure and the resulting higher enthalpy difference in the expansion process. Furthermore, the addition of the regenerator results in the increase of net power output. In the PR-ORC system, the maximum net power output of 4.61 kW is achieved at $P_4$ = 10.7 MPa for pure $CO_2$, while 5.30 kW is obtained at $P_4$ = 10.6 MPa for $CO_2$/R134a mixture. Appendix A supplements detailed experimental results with the thermodynamic properties of each state point based on maximum net power output.

For a fair comparison, the net power output at a certain expansion inlet pressure value of 10 MPa is estimated using a quadratic fitted method based on existing test data. The quadratic fitted results are listed in Table 6. At an expansion inlet pressure of 10 MPa, $CO_2$/R134a provides 16.7% more net power output than pure $CO_2$ for the P-ORC and 23.3% for the PR-ORC. Including the regenerator, the net power output increases by 32.5% for pure $CO_2$ and 40% for $CO_2$/R134a mixture.

Fig. 10 shows the variation in thermal efficiency for pure $CO_2$ and $CO_2$/R134a mixture. For all scenarios thermal efficiency shows an increasing trend with expansion inlet pressure.

For system configurations, PR-ORC offers higher thermal efficiency than P-ORC. Meanwhile, $CO_2$/R134a mixture is capable of achieving higher thermal efficiency than pure $CO_2$ because of its higher pressure ratio. In the PR-ORC, a maximum thermal efficiency of 10.14% occurred at $P_4$ = 10.6 MPa for $CO_2$/R134a mixture; a maximum thermal efficiency of 9.30% occurred at $P_4$ = 10.7 MPa for pure $CO_2$. At the same $P_4$ = 10 MPa shown in Table 6, $CO_2$/R134a mixture achieves an increase in thermal efficiency of 26.5% in the P-ORC and 16.4% in the PR-ORC compared to pure $CO_2$. Adding the regenerator increases the thermal efficiency a total by 43.3% for pure $CO_2$ and 31.9% for $CO_2$/R134a mixture.

Previous studies indicated that $CO_2$ is capable of achieving a good thermal matching in the preheater and the resulting low exergy destruction [11]. The thermal matching and exergy destruction of $CO_2$/R134a mixture is compared with that of pure $CO_2$ below.

Fig. 11(a) shows the exergy destructions of various heat exchangers in the PR-ORC. For both pure $CO_2$ and $CO_2$/R134a mixture, the highest exergy destruction is achieved by the gas heater, followed by the condenser, the regenerator and the preheater. Compared to pure $CO_2$, the $CO_2$/R134a mixture owns higher exergy destructions in the condensers but lower exergy destruction in the gas heater and regenerator. The high exergy destruction in the condensers may be attributable to the poor thermal matching induced by the temperature glide in the condensing process. Furthermore, the difference of the exergy destruction in the regenerator and gas heater between pure $CO_2$ and $CO_2$/R134a mixture can be explained using Fig. 11(b) and (c), in which the log mean temperature differences of heat exchangers, expressed as $\Delta T_{lm}$, are noted. Clearly, $CO_2$/R134a mixture achieves better thermal matching than pure $CO_2$ in the regenerator and the gas heater, as reflected by the $\Delta T_{lm}$. The primary reason for difference in thermal matching is that the peak specific heat of pure $CO_2$ is obtained at the temperature range in which the working fluid absorbs heat from the engine coolant, whereas the peak specific heat of $CO_2$/R134a mixture is achieved at a relatively high temperature (see Fig. 7).

The maximum exergy efficiencies of pure $CO_2$ and the $CO_2$/R134a mixture are 21.24% and 24.34%, respectively, as shown in Fig. 12. At the $P_4$ = 10 MPa presented in Table 6, the $CO_2$/R134a mixture achieves an increase of 20.0% in the P-ORC and 23.7% in the PR-ORC compared to pure $CO_2$. The addition of the regenerator results in an increase in exergy efficiency of 39.1% for pure $CO_2$ and 43.3% for the $CO_2$/R134a mixture.

### 6.3. System performance of $CO_2$/R134a mixture under ambient cooling conditions

As mentioned above, the low critical temperature of $CO_2$ makes it difficult for $CO_2$ to be condensed at ambient cooling sources, which represents the main barrier to using $CO_2$ for engine waste heat recovery. In this section, the performance of $CO_2$/R134a mixture was tested further under ambient cooling conditions (25.2–31.5 °C).

After the refrigerating unit was shut down, the cooling water temperature was increased gradually, as indicated by several parameters, to ensure the steady operation of the ORC system. Fig. 13 shows the variation with time of primary measured parameters after shutdown of the refrigerating unit. The cooling water inlet temperature $T_{c1}$ and working fluid temperature at condenser-2 outlet $T_8$ both rose slowly. The pressure at the condenser-2 outlet $P_8$ increased correspondingly. About 20 min after the refrigerating unit shutdown, the temperature of working fluid $T_8$ reached the critical temperature of 31.1 °C for $CO_2$. After another 7.5 min, the cooling water inlet temperature $T_{c1}$ reached the ambient temperature of 25 °C. During this process, $P_8$ increased from 5.04 to 5.37 MPa.

The liquid height of working fluid tank $H$ and mass flow rate of working fluid $m_f$ are two important indicators for steady operation of the ORC system. The mass flow rate of the working fluid decreased reposefully as cooling water inlet temperature increased. The decreasing trend may be attributable to the decrease in the density of working fluid at the pump inlet caused by the increase of $T_8$. At about 22 min, the system's mass flow rate underwent a sudden decrease and then a rapid return to a normal value. The fluctuation in mass flow rate may reflect the fact that the thermos-physical attributes of CO2 show drastic and fast changes in the neighborhood of its critical point.

The experimental results described above confirm that an ORC system using the $CO_2$/R134a mixture is capable of operating steadily under ambient cooling conditions, meaning that the $CO_2$/R134a mixture can expand the range of condensation temperatures and alleviate

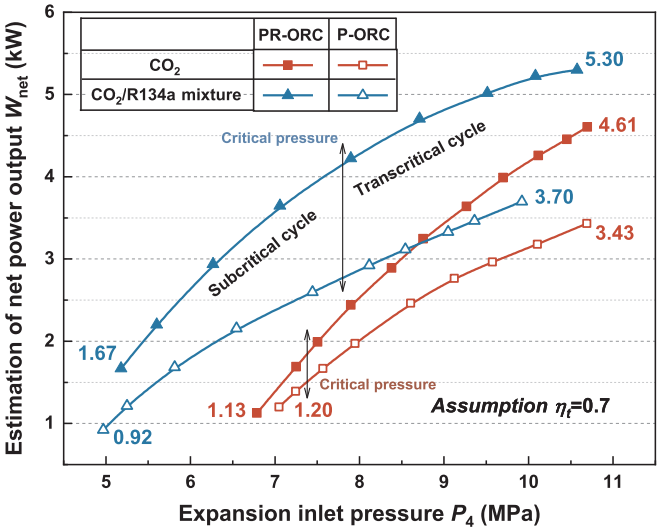


**Fig. 9.** Estimation of net power output for pure $CO_2$ and $CO_2$/R134a mixture in the PR-ORC and the P-ORC.

**Table 6**
Fitted results of net power output estimation, thermal efficiency and exergy efficiency at an expansion inlet pressure of 10 MPa.

| | $CO_2$/R134a mixture | | Pure $CO_2$ | |
|---|---|---|---|---|
| | P-ORC | PR-ORC | P-ORC | PR-ORC |
| Net power output estimation (kW) | 3.70 | 5.18 | 3.17 | 4.20 |
| Thermal efficiency (%) | 7.45 | 9.83 | 5.89 | 8.44 |
| Exergy efficiency (%) | 16.59 | 23.77 | 13.82 | 19.22 |

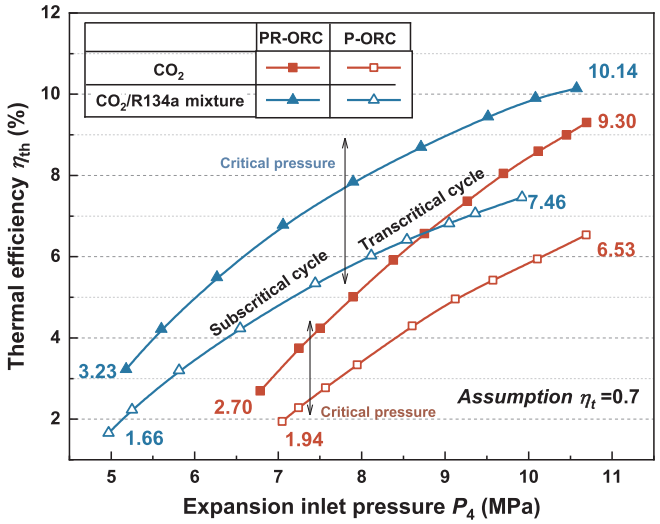


**Fig. 10.** Variation in thermal efficiencies for pure $CO_2$ and $CO_2$/R134a mixture in the PR-ORC and the P-ORC.

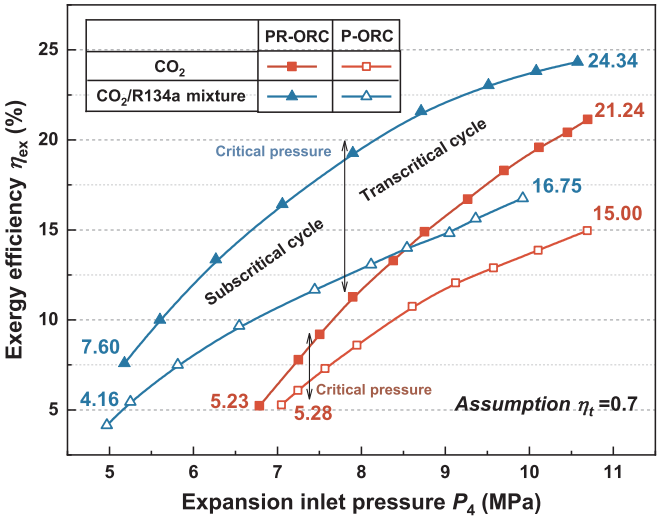


**Fig. 12.** Variation in exergy efficiencies for pure $CO_2$ and $CO_2$/R134a mixture in the PR-ORC and the P-ORC.

the low-temperature condensation issue encountered with $CO_2$. Hence, the $CO_2$/R134a mixture exhibits a high technical potential for providing engine waste heat recovery.

The experiment under ambient cooling conditions was performed using the same experimental strategy as described above. The steady state experimental points used for system performance estimation are presented in Table 7.

Fig. 14 shows the variation in net power output estimations under ambient cooling conditions. The figure shows that net power output estimations ranging from 0.42 to 2.88 kW can be obtained by P-ORC; they vary in the range of 0.66 to 3.54 kW for PR-ORC.

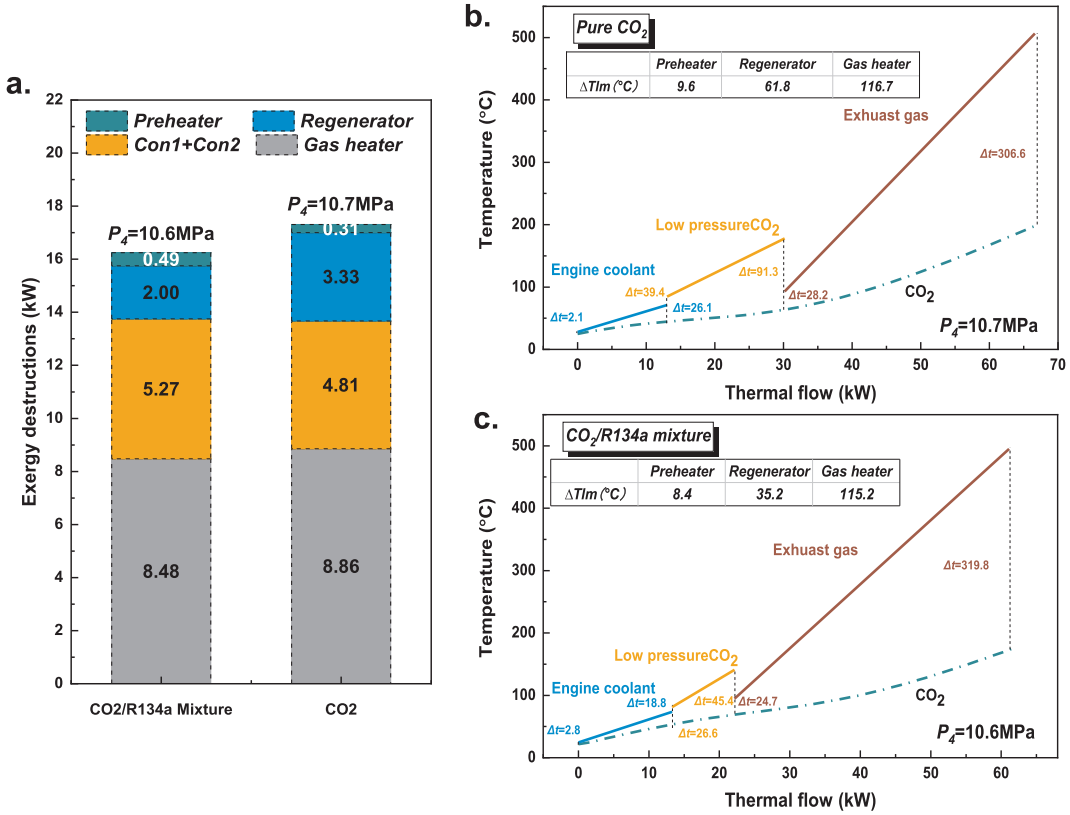


**Fig. 11.** (a) Exergy destructions of various heat exchangers for pure $CO_2$ and $CO_2$/R134a mixture in the PR-ORC; (b) *T-Q* plot of heating process for pure $CO_2$; (c) *T-Q* plot of heating process for $CO_2$/R134a mixture.

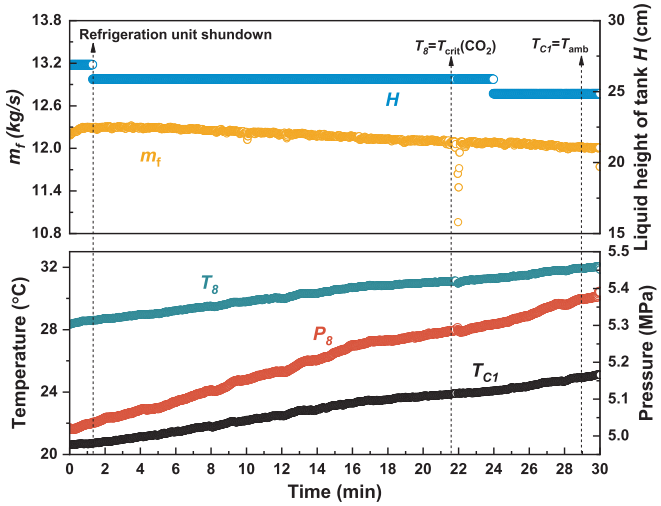


**Fig. 13.** Change in primary measured parameters after shutdown of the refrigerator unit.

**Table 7**
Steady state experimental points used for system performance estimation.

| | | | | | | | | | | |
|---|---|---|---|---|---|---|---|---|---|---|
| *P-ORC* | | | | | | | | | | |
| $P_4$/(MPa) | 5.95 | 6.11 | 6.31 | 6.70 | 7.14 | 7.81 | 8.87 | 9.78 | 10.23 | 10.57 |
| $P_5$/(MPa) | 5.46 | 5.49 | 5.50 | 5.50 | 5.50 | 5.51 | 5.52 | 5.51 | 5.51 | 5.55 |
| *PR-ORC* | | | | | | | | | | |
| $P_4$/(MPa) | 6.42 | 6.58 | 6.82 | 7.17 | 7.52 | 7.90 | 8.51 | 9.26 | 10.15 | 10.53 |
| $P_5$/(MPa) | 5.82 | 5.84 | 5.85 | 5.88 | 5.89 | 5.89 | 5.91 | 5.91 | 5.91 | 5.93 |

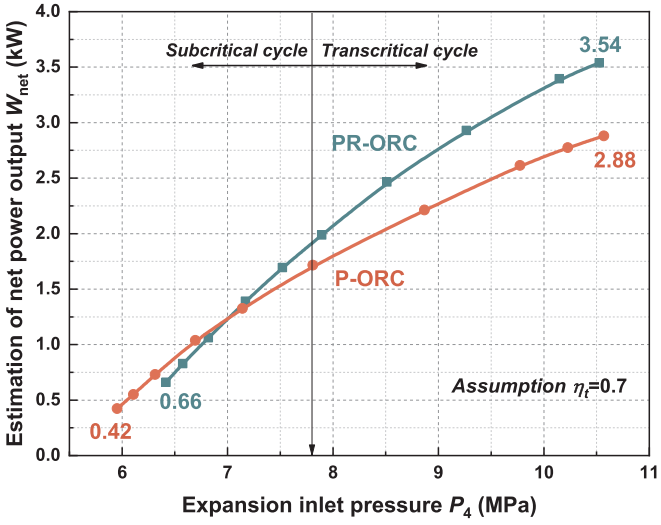


**Fig. 14.** Variation in net power output under ambient cooling conditions.

Fig. 14 indicates that PR-ORC provides higher net power output than P-ORC when the expansion inlet pressure exceeds 7.0 MPa, a result that is not realized at a low expansion inlet pressure. This result is quite different from the abovementioned comparative experimental results with pure $CO_2$. The lower net power obtained by the PR-ORC at low pressure is attributed to the decrease in heat absorption as depicted in Fig. 15. The increase in the expansion outlet pressure leads to a decrease of the pressure ratio and a resulting higher expansion outlet temperature. Thus, the PR-ORC system absorbs more heat in the regenerator while withdrawing less heat from exhaust gas. The high expansion outlet pressure also reduces the amount of heat absorption in the preheater.

Fig. 16 shows the thermal efficiency and exergy efficiency of both the P-ORC and the PR-ORC. The trend in thermal efficiency is a combination of the net power output estimation and the amount of heat absorption, as discussed above. The maximum thermal efficiency of the PR-ORC is 7.97%, achieved at $P_4$ = 10.5 MPa. Maximum thermal efficiency of the P-ORC is 6.25% at 10.6 MPa. The exergy efficiency shown in Fig. 16(b) shows the same trend as the net power output, which means the net power output is critical in influencing the exergy efficiency. The maximum exergy efficiencies of the PR-ORC and the P-ORC are 16.40% and 12.95%, respectively.

Combined with the ORC system, the thermal efficiency of the diesel engine would be improved. The thermal efficiencies of the original diesel engine and the diesel engine combined with the ORC system are depicted in Fig. 17. Under an ambient cooling source, the maximum improvement in thermal efficiency is 1.5% for the P-ORC and 1.9% for the PR-ORC. Hence, the thermal efficiency of the combined diesel engine-ORC system can reach 38.9% versus an original diesel engine thermal efficiency of 37%.

## 7. Conclusion

A preliminary experimental comparison of pure $CO_2$ and a $CO_2$/R134a mixture (0.6/0.4 on a mass basis) for engine waste heat recovery was performed using an expansion valve. Measured operating parameters and system performance were compared under the preheating Organic Rankine Cycle (P-ORC) and the preheating regenerative Organic Rankine Cycle (PR-ORC). In addition, the application potential of $CO_2$/R134a (0.6/0.4) mixture for engine waste heat recovery was tested under ambient cooling conditions. The primary conclusions of this work are given below.

(1) For the PR-ORC, as the expansion inlet pressure increases, the expansion inlet temperature increases from 181.6 °C to about 200 °C for $CO_2$, while the expansion inlet temperature of $CO_2$/R134a mixture decreases from 188.5 °C to 175.2 °C.
(2) $CO_2$/R134a (0.6/0.4) mixture exhibits better system performance than pure $CO_2$. For the PR-ORC using $CO_2$/R134a (0.6/0.4) mixture, assuming a turbine isentropic efficiency of 0.7, the net power output estimation, thermal efficiency and exergy efficiency reach 5.30 kW, 10.14% and 24.34%, respectively. At the same expansion inlet pressure of 10 MPa, the net power output estimation, thermal efficiency and exergy efficiency using $CO_2$/R134a mixture achieve an increase of 23.3%, 16.4% and 23.7%, respectively, compared with using pure $CO_2$ as working fluid.
(3) The PR-ORC performs better than the P-ORC for both pure $CO_2$ and

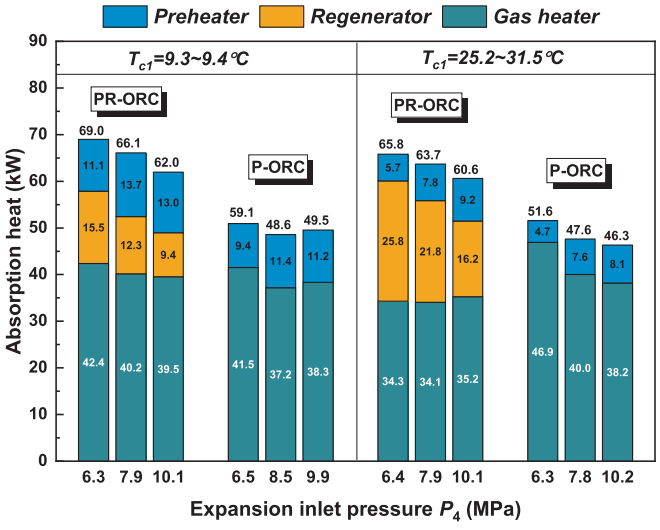


**Fig. 15.** Amount of heat absorption in the P-ORC and the PR-ORC.

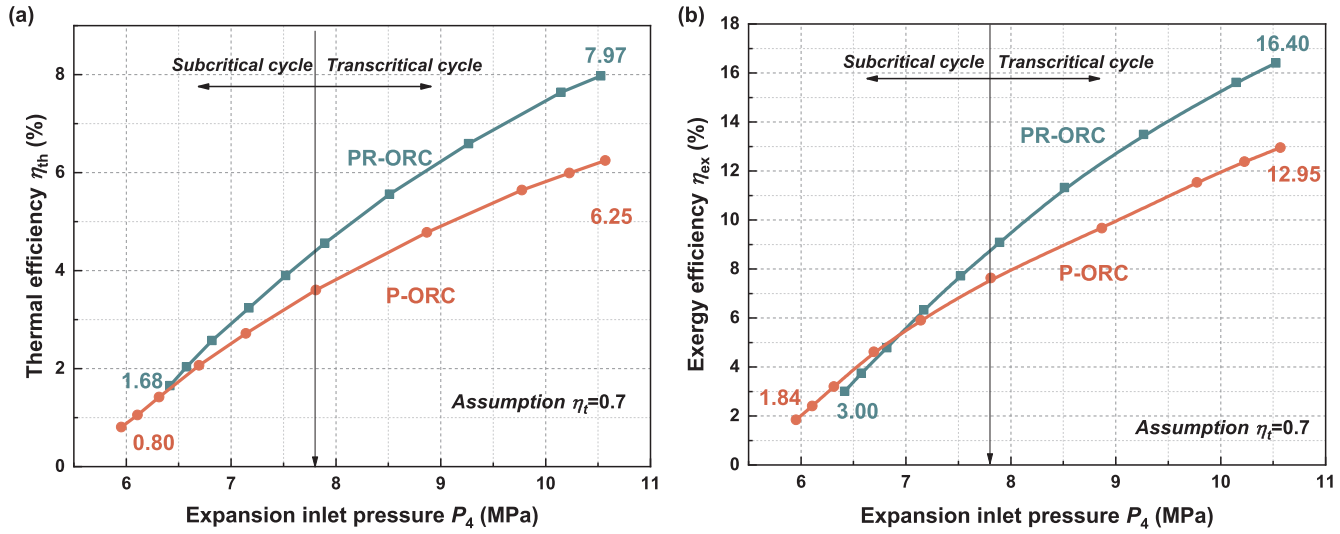


**Fig. 16.** Performance of the P-ORC and the PR-ORC: (a) thermal efficiency; (b) exergy efficiency.

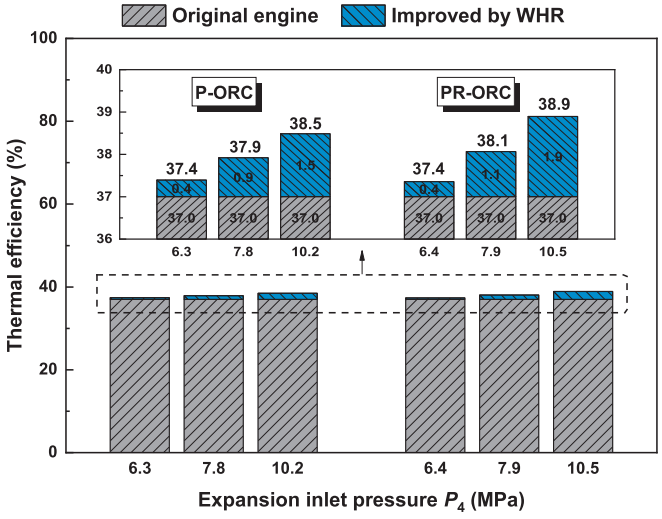


**Fig. 17.** Thermal efficiency of diesel engine and combined diesel engine-ORC combined system.

$CO_2$/R134a mixture. By adding the regenerator for the case of $CO_2$/R134a (0.6/0.4) mixture, net power output estimation, thermal efficiency and exergy efficiency increase by 40%, 31.9% and 43.3%, respectively.

(4) In the heating process, $CO_2$/R134a (0.6/0.4) mixture shows better thermal matching in the regenerator and the gas heater compared with pure $CO_2$. We attribute this result to the its high temperature range for the peak specific heat. $CO_2$/R134a (0.6/0.4) mixture demonstrates poor thermal matching in the cooling process because of its temperature glide.

(5) Experiments showed that the ORC system using $CO_2$/R134a mixture (0.6/0.4) is capable of operating steadily under ambient cooling conditions. Results demonstrates that $CO_2$/R134a mixture can expand the range of condensation temperature and thus alleviate the low-temperature condensation issue encountered with $CO_2$. Under ambient cooling conditions, the thermal efficiency of a diesel engine is expected to be improved by 1.9% using $CO_2$/R134a (0.6/0.4) mixture.

## Declaration of Competing Interest

None.

## Acknowledgement

The authors would like to acknowledge the Key Technologies Research and Development Program of China (2017YFE0102800) for grants and supports. Financial support from China Scholarship Council (CSC) to the first author also is gratefully acknowledged.

The U.S. authors recognize Lawrence Berkeley National Laboratory's support from Department of Energy – The United States under Contract No. DE-AC02-05CH11231 and supports from the Energy Foundation. The U.S. Government retains a non-exclusive, paid-up, irrevocable, world-wide license to publish or reproduce the published form of this manuscript, or allow others to do so, for U.S. Government purposes.

## Appendix A

Detailed experimental results along with the thermodynamic properties of each state point based on maximum net power output.

| Point | $T$/(°C) | $P$/(MPa) | $h$/(kJ/kg) | $s$/(kJ/kg K) |
|---|---|---|---|---|
| *Pure $CO_2$* | | | | |
| 1 | 25.9 | 10.74 | 257.2 | 1.1709 |
| 2 | 41.1 | 10.73 | 309.6 | 1.3416 |
| 3 | 64.9 | 10.71 | 426.8 | 1.7028 |
| 4 | 200.0 | 10.69 | 629.9 | 2.2194 |
| 5 | 178.0 | 5.98 | 622.8 | 2.3053 |
| 6 | 84.6 | 5.95 | 516.3 | 2.0410 |
| 7 | 21.3 | 5.94 | 260.1 | 1.2013 |

| | | | | |
|---|---|---|---|---|
| 8 | 21.0 | 5.93 | 258.9 | 1.1971 |
| 9 | 19.3 | 5.93 | 251.9 | 1.1734 |
| *$CO_2$/R134a mixture* | | | | |
| 1 | 21.9 | 10.64 | 238.7 | 1.1081 |
| 2 | 44.6 | 10.61 | 285.2 | 1.2602 |
| 3 | 70.0 | 10.62 | 357.2 | 1.4774 |
| 4 | 175.2 | 10.57 | 566.2 | 2.0234 |
| 5 | 141.0 | 3.96 | 559.8 | 2.1333 |
| 6 | 81.3 | 3.93 | 492.5 | 1.9587 |
| 7 | 23.9 | 3.92 | 310.8 | 1.3773 |
| 8 | 17.1 | 3.90 | 233.8 | 1.1153 |
| 9 | 16.3 | 3.90 | 232.1 | 1.1094 |

## References


[1] International Energy Agency, World Energy Outlook 2017. 2017.11. https://www.iea.org/weo2017/.

[2] Shu G, Yu G, Tian H, Wei H, Liang X, Huang Z. Multi-approach evaluations of a cascade-Organic Rankine Cycle (C-ORC) system driven by diesel engine waste heat: Part A – Thermodynamic evaluations. Energy Convers Manage 2016;108:579–95.

[3] Villani M, Tribioli L. Comparison of different layouts for the integration of an organic Rankine cycle unit in electrified powertrains of heavy duty Diesel trucks. Energy Convers Manage 2019;187:248–61.

[4] Yang M-H. Payback period investigation of the organic Rankine cycle with mixed working fluids to recover waste heat from the exhaust gas of a large marine diesel engine. Energy Convers Manage 2018;162:189–202.

[5] Soffiato M, Frangopoulos CA, Manente G, Rech S, Lazzaretto A. Design optimization of ORC systems for waste heat recovery on board a LNG carrier. Energy Convers Manage 2015;92:523–34.

[6] Wang X, Shu G, Tian H, Feng W, Liu P, Li X. Effect factors of part-load performance for various Organic Rankine cycles using in engine waste heat recovery. Energy Convers Manage 2018;174:504–15.

[7] Harby K. Hydrocarbons and their mixtures as alternatives to environmental unfriendly halogenated refrigerants: an updated overview. Renew Sustain Energy Rev 2017;73:1247–64.

[8] UNEP. Handbook for international treaties for protection of the ozone layers. 6th ed. Nairobi, Kenya: United Nation Environment Program (UNEP); 2003.

[9] Shu G, Shi L, Tian H, Li X, Huang G, Chang L. An improved CO2-based transcritical Rankine cycle (CTRC) used for engine waste heat recovery. Appl Energy 2016;176:171–82.

[10] Shu G, Shi L, Tian H, Deng S, Li X, Chang L. Configurations selection maps of CO2-based transcritical Rankine cycle (CTRC) for thermal energy management of engine waste heat. Appl Energy 2016.

[11] Shi L, Shu G, Tian H, Huang G, Chen T, Li X, et al. Experimental comparison between four CO2-based transcritical Rankine cycle (CTRC) systems for engine waste heat recovery. Energy Convers Manage 2017;150:159–71.

[12] Song J, Li X-S, Ren X-D, Gu C-W. Performance improvement of a preheating supercritical CO2 (S-CO2) cycle based system for engine waste heat recovery. Energy Convers Manage 2018;161:225–33.

[13] Irwin L, Le Moullec Y. Turbines can use $CO_2$ to cut $CO_2$. Science 2017;356(6340):805–6.

[14] Musgrove GO, Shiferaw D, Sullivan S, Portnoff LCM. Tutorial: Heat Exchangers for Supercritical CO2 Power Cycle Applications; 2016.

[15] Choi BC. Thermodynamic analysis of a transcritical CO 2 heat recovery system with 2-stage reheat applied to cooling water of internal combustion engine for propulsion of the 6800 TEU container ship. Energy 2016;107:532–41.

[16] Wang SS, Wu C, Li J. Exergoeconomic analysis and optimization of single-pressure single-stage and multi-stage CO2 transcritical power cycles for engine waste heat recovery: a comparative study. Energy 2018;142:559–77.

[17] Persichilli M, Held T, Hostler S, Zdankiewicz E, Klapp D. Transforming waste heat to power through development of a CO2-based-power cycle. Electric Power Expo 2011:10–2.

[18] Li X, Shu G, Tian H, Shi L, Huang G, Chen T, et al. Preliminary tests on dynamic characteristics of a CO2 transcritical power cycle using an expansion valve in engine waste heat recovery. Energy 2017;140:696–707.

[19] Shi L, Shu G, Tian H, Chen T, Liu P, Li L. Dynamic tests of CO2-Based waste heat recovery system with preheating process. Energy 2019;171:270–83.

[20] Li X, Shu G, Tian H, Huang G, Liu P, Wang X, et al. Experimental comparison of dynamic responses of $CO_2$ transcritical power cycle systems used for engine waste heat recovery. Energy Convers Manage 2018;161:254–65.

[21] Garg P, Kumar P, Srinivasan K, Dutta P. Evaluation of carbon dioxide blends with isopentane and propane as working fluids for organic Rankine cycles. Appl Therm Eng 2013;52;(2):439–48.

[22] Shu G, Yu Z, Tian H, Liu P, Xu Z. Potential of the transcritical Rankine cycle using CO2-based binary zeotropic mixtures for engine's waste heat recovery. Energy Convers Manage 2018;174:668–85.

[23] Dai B, Li M, Ma Y. Thermodynamic analysis of carbon dioxide blends with low GWP (global warming potential) working fluids-based transcritical Rankine cycles for low-grade heat energy recovery. Energy 2014;64(1):942–52.

[24] Wu C, Wang SS, Jiang X, Li J. Thermodynamic analysis and performance optimization of transcritical power cycles using CO2-based binary zeotropic mixtures as working fluids for geothermal power plants. Appl Therm Eng 2017;115:292–304.

[25] Pan L, Wei X, Shi W. Performance analysis of a zeotropic mixture (R290/CO2) for trans-critical power cycle. Chinese J Chem Eng 2015;23(3):572–7.

[26] Yin H, Sabau AS, Conklin JC, Mcfarlane J, Qualls AL. Mixtures of SF6–CO2 as working fluids for geothermal power plants. Appl Energy 2013;106(11):243–53.

[27] Bamorovat Abadi G, Kim KC. Investigation of organic Rankine cycles with zeotropic mixtures as a working fluid: advantages and issues. Renew Sustain Energy Rev 2017;73:1000–13.

[28] Wang JL, Zhao L, Wang XD. A comparative study of pure and zeotropic mixtures in low-temperature solar Rankine cycle. Appl Energy 2010;87(11):3366–73.

[29] Bamorovat Abadi G, Yun E, Kim KC. Experimental study of a 1 kw organic Rankine cycle with a zeotropic mixture of R245fa/R134a. Energy 2015;93:2363–73.

[30] Jung HC, Taylor L, Krumdieck S. An experimental and modelling study of a 1kW organic Rankine cycle unit with mixture working fluid. Energy 2015;81:601–14.

[31] Li T, Zhu J, Fu W, Hu K. Experimental comparison of R245fa and R245fa/R601a for organic Rankine cycle using scroll expander: organic Rankine cycle using scroll expander. Int. J. Energy Res 2015;39(2):202–14. https://doi.org/10.1002/er.v39.210.1002/er.3228.

[32] Pang K-C, Chen S-C, Hung T-C, Feng Y-Q, Yang S-C, Wong K-W, et al. Experimental study on organic Rankine cycle utilizing R245fa, R123 and their mixtures to investigate the maximum power generation from low-grade heat. Energy 2017;133:636–51.

[33] Meng Z, Zhang H, Lei M, Qin Y, Qiu J. Performance of low GWP R1234yf/R134a mixture asa replacement for R134a in automotive air conditioning systems. Int J Heat Mass Transf 2018;116:362–70.

[34] Uusitalo A, Honkatukia J, Turunen-Saaresti T. Evaluation of a small-scale waste heat recovery organic Rankine cycle. Appl Energy 2017;192:146–58.

[35] Brun K, Friedman P, Dennis R. Fundamentals and applications of supercritical carbon dioxide (sCO2) based power cycles. Woodhead Publishing; 2017.